6. S. Jin *et al.*, *Nano Lett.* **4**, 915 (2004).
7. R. P. Sear *et al.*, *Phys. Rev. E* **59**, R6255 (1999).
8. M. Diehl *et al.*, *Angew. Chem. Int. Ed. Engl.* **41**, 353 (2002).
9. N. A. Melosh *et al.*, *Science* **300**, 112 (2003); published online 13 March 2003 (10.1126/science.1081940).
10. P. J. Kuekes, R. S. Williams, U.S. Patent 6,256,767 (3 July 2001).
11. A. DeHon, P. Lincoln, J. Savage, *IEEE Trans. Nanotechnol.* **2**, 165 (2003).
12. J. Heath, P. Kuekes, G. Snider, R. S. Williams, *Science* **280**, 1716 (1998).
13. R. P. Feynman, *Lectures in Computation*, A. J. G. Hey, R. W. Allen, Eds. (Addison-Wesley, Menlo Park, CA, 1996).
14. See supporting data on *Science* Online.
15. M. S. Gudiksen *et al.*, *Nature* **415**, 617 (2002).
16. Y. Wu, R. Fan, P. Yang, *Nano Lett.* **2**, 83 (2002).
17. M. T. Bjork *et al.*, *Nano Lett.* **2**, 87 (2002).
18. Z. Zhong *et al.*, *Science* **302**, 1377 (2003).
19. S. Y. Chou, P. R. Krauss, P. J. Renstrom, *Science* **272**, 85 (1996).
20. Y. Chen *et al.*, *Appl. Phys. Lett.* **82**, 1610 (2003).
21. G. D. Wilk, R. M. Wallace, *Appl. Phys. Lett.* **74**, 2854 (1999).
22. J. Hergenrother *et al.*, in *Electron Devices Meeting, 2001. IEDM Technical Digest International* (IEEE, Piscataway, NJ, 2001), pp. 3.1.1–3.1.4.
23. M. Quevedo-Lopez *et al.*, *Appl. Phys. Lett.* **79**, 4192 (2001).
24. D. M. Hausmann, E. Kim, J. Becker, R. G. Gordon, *Chem. Mater.* **14**, 4350 (2002).
25. A. Javey *et al.*, *Nat. Mater.* **1**, 241 (2002).
26. A. Javey *et al.*, *Nano Lett.* **4**, 447 (2004).
27. D. Wang *et al.*, *Appl. Phys. Lett.* **83**, 2432 (2003).
28. R. Beckman *et al.*, *J. Appl. Phys.* **96**, 5921 (2004).
29. These comparisons are based on measurements of the normalized current through the selected and deselected nanowires, rather than absolute current values.
30. R. Puthenkoviliakam, M. Sawker, J. P. Chang, *Appl. Phys. Lett.* **86**, 202902 (2005).
31. H. Yu *et al.*, *J. Phys. Chem. B* **109**, 671 (2005).
32. W. J. Royea, A. Juang, N. S. Lewis, *Appl. Phys. Lett.* **77**, 1988 (2000).
33. L. Peters, *Semiconductor International*, September 1998 (available at www.reed-electronics.com/semiconductor/archive/1998).
34. Y. Bunimovich *et al.*, *Langmuir* **20**, 10630 (2004).
35. L. Hood, J. R. Heath, M. E. Phelps, B. Lin, *Science* **306**, 640 (2004).

36. Supported by the Defense Advanced Research Projects Agency (DARPA) Moletronics Program and by the MARCO Center for Advanced Materials and Devices.

Supporting Online Material

www.sciencemag.org/cgi/content/full/1114757/DC1
Materials and Methods
SOM Text
Figs. S1 to S6
References

12 May 2005; accepted 21 September 2005
Published online 29 September 2005
10.1126/science.1114757
Include this information when citing this paper.

Visualization of the Molecular Jahn-Teller Effect in an Insulating K_4C_{60} Monolayer

A. Wachowiak, R. Yamachika, K. H. Khoo, Y. Wang, M. Grobis, D.-H. Lee, Steven G. Louie, M. F. Crommie*

We present a low-temperature scanning tunneling microscopy (STM) study of K_xC_{60} monolayers on Au(111) for $3 \leq x \leq 4$. The STM spectrum evolves from one that is characteristic of a metal at $x = 3$ to one that is characteristic of an insulator at $x = 4$. This electronic transition is accompanied by a dramatic structural rearrangement of the C_{60} molecules. The Jahn-Teller effect, a charge-induced mechanical deformation of molecular structure, is directly visualized in the K_4C_{60} monolayer at the single-molecule level. These results, along with theoretical analyses, provide strong evidence that the transition from metal to insulator in K_xC_{60} monolayers is caused by the Jahn-Teller effect.

Unlike atoms in an elemental solid, the building blocks of a molecular solid are more susceptible to tuning. C_{60}-based bulk solids, for example, can be tuned between metallic (*1*), insulating (*2*, *3*), and superconducting (*4*) states by changing the charge state and/or local environment of the constituent molecules. The cooperative interplay between molecular electronic and lattice degrees of freedom (the latter referring to intramolecular and intermolecular atomic displacements) is particularly important in fullerenes, because the energy scale of their electron-lattice interaction is comparable to their electronic bandwidths (*5*, *6*). As a result, small changes in properties such as intermolecular hybridization, intramolecular charging energy, and Jahn-Teller (JT) distortions (*7*) can tip these systems from one side of the metal-insulator divide to the other. This behavior has been studied extensively in C_{60}-based systems (*8*–*11*), but the role played by the JT effect, in which degenerate molecular electronic levels are split due to a spontaneous charge-induced structural deformation (*7*), is still under debate (*11*–*18*).

We report a cryogenic (temperature $T = 7$ K) scanning tunneling microscopy (STM) study of a single monolayer (ML) of potassium-doped C_{60} (K_xC_{60}) on Au(111), which shows that the JT effect plays a central role in driving the K_xC_{60} ML from a metal at $x = 3$ to an insulator at $x = 4$. This progress is made possible by our ability to directly image the influence of a JT distortion on intramolecular electronic wave functions.

The driving force for the JT effect is a lowering of occupied electronic levels coincident with a raising of empty ones, which reduces the total energy. The symmetry of electronic wave functions in a JT distorted molecule bears the imprint of the distortion itself and is very different for occupied and empty levels, in contrast with undistorted molecules. By comparing STM images of the intramolecular local density of states (LDOS) above and below the Fermi energy (E_F), we can determine the presence or absence of a JT distortion.

The charge state of C_{60} molecules in the K_xC_{60} ML was controlled through the local K concentration (each K atom donates approximately one electron to the physisorbed C_{60} molecules) (*5*, *19*, *20*). Upon bias reversal, the LDOS images changed dramatically for the $x = 4$ system but remained the same for $x = 3$, suggesting that a substantial JT distortion was present in the former and absent in the latter. We back this conclusion with ab initio electronic structure calculations that show our STM images are well-matched by the theoretical LDOS of a molecule undergoing a JT distortion. This combined evidence not only prompts us to conclude that a static JT distortion is the trigger of the insulating behavior in K_4C_{60} MLs but also allows us to determine the nature of the distortion.

The local structure of K-doped C_{60} MLs can be seen in the STM data of Fig. 1 (*21*). At $x = 3$, K_xC_{60} exhibits a triangular lattice backbone with a "bright molecule" supermodulation (Fig. 1A), reflecting a K-induced surface reconstruction. The exact form of the supermodulation varies across the K_3C_{60} surface and exhibits pronounced disorder in some regions, whereas it disappears altogether in others. Metallic dI/dV spectra, where I is current and V is voltage (Fig. 1D), are observed regardless of the details of the supermodulation. At $x = 4$, the K_xC_{60} ML undergoes a dramatic restructuring that transforms the underlying triangular backbone into a nearly rectangular structure with four molecules per unit cell (Fig. 1C). This structure is free of supermodulation and is far more ordered than are the $x = 3$ structures. The dI/dV spectrum for the $x = 4$ phase exhibits an energy gap of 200 ± 20 mV that is roughly symmetrical about E_F (see Fig. 1E). When the average K content (x) falls between 3 and 4, the system is an inhomogeneous mixture of the two phases (Fig. 1B). The spatial inhomogeneity is reflected both in the dI/dV spectra and structurally.

Department of Physics, University of California at Berkeley, Berkeley, CA 94720–7300, USA, and Material Sciences Division, Lawrence Berkeley Laboratory, Berkeley, CA 94720–7300, USA.

*To whom correspondence should be addressed. E-mail: crommie@berkeley.edu

The difference in electronic properties between the $x = 3$ and $x = 4$ phases can be seen by comparing real-space images of the filled and empty states straddling E_F (Figs. 2 and 3). A collection of *dI*/*dV* spectra measured at different points within a 3 nm × 3 nm region of the K_3C_{60} ML (Fig. 2C) shows some variability, but all of the spectra reveal a similar peak near E_F ($V = 0$). Topographic images at $V = -100$ mV (filled states) and $V = +100$ mV (empty states) for the same patch of K_3C_{60} surface (Fig. 2, A and B) show little change upon bias reversal, which is indicative of undistorted molecules and a continuous metallic LDOS. Data for the K_4C_{60} phase (Fig. 3C) show that instead of a peak at E_F, a 200-mV energy gap exists. Most striking, however, is the difference in the topographic images associated with filled and empty states (measured at $V = -100$ mV and $+100$ mV, respectively). Filled-state images (Fig. 3A) show that each C_{60} molecule is bisected by a single nodal line (i.e., a dark stripe), which implies the presence of a similar feature in the molecular LDOS. Empty-state images (Fig. 3B), however, display an additional nodal line on each molecule that is rotated by 90° with respect to the node seen in the filled-state image.

We argue that the dramatic difference in the filled- and empty-state topography of Fig. 3 is a manifestation of the JT distortion. When four extra electrons are added, a C_{60} molecule is expected to undergo a JT distortion whereby the three degenerate lowest unoccupied molecular orbital (LUMO) levels split into a group of twofold degenerate levels (excluding spin mutiplicity) at lower energy and one nondegenerate level at higher energy (*22*–*24*). The four extra electrons are accommodated by the two lowered energy levels, making the distortion energetically favorable. The shifting of the electronic levels by the molecular distortion implies an intimate relation between the electronic wave functions and the symmetry of the JT distortion.

To determine that relation, we compared our STM topographic images with calculated molecular LDOS by using density functional theory (DFT) with ab initio pseudopotential in a local orbital basis. Different locally stable distorted structures for isolated C_{60}^{4-} were found by total energy minimization. Their electronic LDOSs were then compared to our STM results and the best-fit structure selected. Apart from using an improved basis set (*25*), a finer real space grid (0.1 Å mesh), and excluding the surface, details of the calculation method are similar to those in (*26*). Guided by symmetry considerations (*22*–*24*), the molecule was given a small initial distortion having either D_{2h}, D_{3d}, or D_{5d} symmetry, and then allowed to relax to minimize the energy. The resulting displacements can be resolved in terms of the H_g and A_g phonon modes (H_g and A_g are symmetry classes that have even symmetry). The lowest-energy deformation for each of these symmetry channels shows an essentially identical total-energy reduction from the undistorted structure of 0.3 eV per molecule. In all three cases, the molecular JT distortion splits the LUMO manifold by 0.11 eV into doubly degenerate occupied levels and a single unoccupied level. However, only the D_{2h} distortion results in electronic wave functions that match the STM data (supporting online text). Therefore, we believe that this particular distortion is stabilized in the K_4C_{60} ML.

The calculated D_{2h} distortion of the C_{60} cage (Fig. 4, A and B) creates an oblate spheroid, with the short axis along the y direction of the figure. Most of the bond dis-

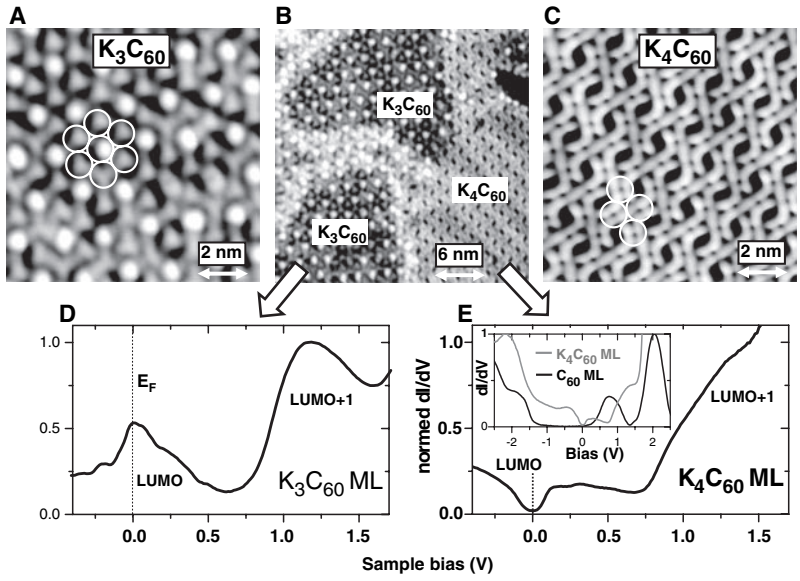

Fig. 1. STM images for K_xC_{60} ML on Au(111), $3 \leq x \leq 4$. (**A**) $x = 3$, single phase ($V = 0.1$ V, $I = 20$ pA, 10 × 10 nm²). (**B**) $x = 3.5$, mixed phase ($V = 0.5$ V, $I = 10$ pA, 25 × 25 nm²). (**C**) $x = 4$, single phase ($V = 0.2$ V, $I = 10$ pA, 10 × 10 nm²). Single molecules are marked by circles. (**D**) Spatially averaged *dI*/*dV* spectrum measured for K_3C_{60} shows metallic behavior. (**E**) Spatially averaged *dI*/*dV* spectrum measured for K_4C_{60} shows energy gap at E_F. The inset shows spatially averaged *dI*/*dV* spectra for a bare C_{60} ML and a K_4C_{60} ML over wider energy range. The spectra shown in (D) and (E) were obtained by spatially averaging over an area of 5 × 5 nm². [All spectra are normalized to the peak value of the LUMO+1 or the highest unoccupied molecular orbital (HOMO).]

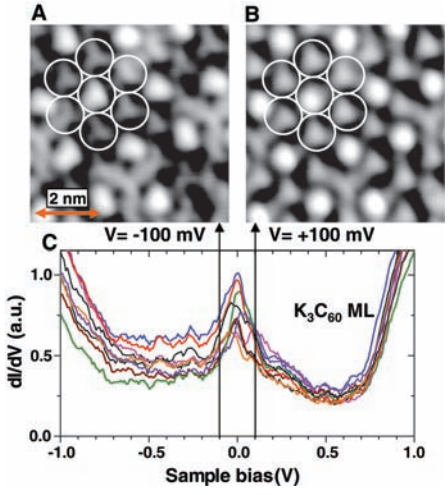

Fig. 2. Energy-dependent STM topographs of same region of K_3C_{60} ML. (**A**) Filled states ($V = -0.10$ V, $I = 20$ pA, 6 × 6 nm²). (**B**) Empty states ($V = +0.10$ V, $I = 20$ pA). Single molecules are marked by circles. (**C**) Spatial variation of *dI*/*dV* spectra measured at different positions in K_3C_{60} ML.

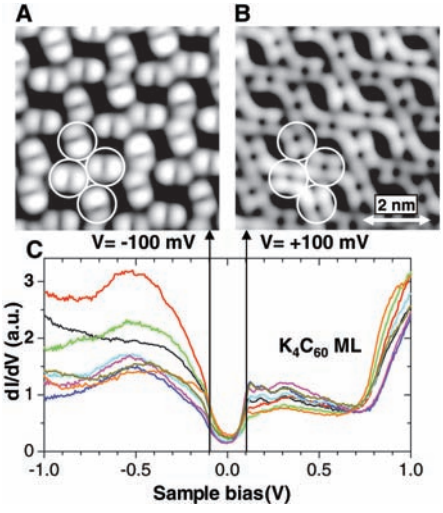

Fig. 3. Energy-dependent STM topographs of same region of K_4C_{60} ML. (**A**) Filled states ($V = -0.10$ V, $I = 10$ pA, 6 × 6 nm²). (**B**) Empty states ($V = +0.10$ V, $I = 10$ pA). The characteristic molecular structure above E_F does not change over the bias range $+0.10$ V to $+0.6$ V, whereas the one below E_F does not change over the bias range -0.10 V to -0.7 V. Single molecules are marked by circles. (**C**) Spatial variation of *dI*/*dV* spectra measured at different positions in K_4C_{60} ML. a.u., arbitrary units.

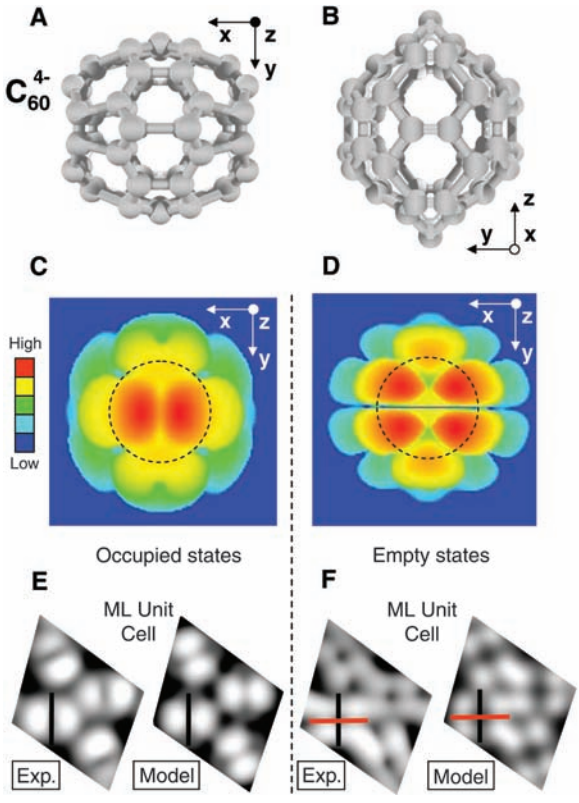

Fig. 4. Results of DFT calculation of isolated C_{60}^{4-} molecule. (**A**) Top view and (**B**) side view of the JT distorted C_{60}^{4-} configuration having D_{2h} symmetry (nuclear displacements are exaggerated by a factor of 30 for viewing). The proposed orientation corresponds to the Au surface parallel to the *xy* plane of the figure. (**C** and **D**) Two-dimensional projection of C_{60}^{4-} isosurface showing highest filled-state and lowest empty-state LDOS for JT split levels at ~3 Å outward from carbon centers. Regions within the dashed circles are preferentially imaged in ML topographs because of finite tip size. (**E** and **F**) STM data for a K_4C_{60} ML unit cell compared with a simulated unit cell obtained from the circled regions of (C) and (D) arranged in ML configuration for filled and empty states. Locations of nodal lines are marked in black and red. Exp., experimental.

tortion occurs in the equatorial *xz* plane. The resulting "isosurfaces" of the LDOS of the energy-split states (plot of $\{\mathbf{x}\}$ with $\Sigma_i \Psi_i(\mathbf{x})\Psi_i(\mathbf{x})^* = C$, where $\mathbf{x}$ is the position vector, Ψ is the wave function, i ranges over degenerate eigenstates at a particular energy, and C is a constant) can be seen in Fig. 4, C and D, for the unique orientation that fits our experimental data (here the Au surface lies in the *xy* plane of the figure). The most pronounced feature in the calculated LDOS of the highest occupied C_{60}^{4-} level (Fig. 4C) is a strong linear depression that bisects the topmost region of the LDOS into two bright areas. The lowest empty state LDOS (Fig. 4D) is similar to the occupied LDOS, except for the addition of a pronounced nodal plane that lies at an angle of 90° from the linear depression seen in the occupied LDOS. This new node lies exactly in the *xz* equatorial plane, where the greatest JT-induced changes in bond length occur, thus marking the spatial location of the JT distortion in the molecular local-electron spectral function. Simulated ML topographs (Fig. 4, E and F) using the results of Fig. 4, C and D, are in good agreement with experimentally observed energy-resolved K_4C_{60} topography. Empty-state imaging of the K_4C_{60} ML thus allows us to directly determine the spatial location of the JT distorted equatorial plane for each individual C_{60} molecule.

Our results provide strong evidence that JT distortion plays a central role in causing the strikingly different electronic properties of $x = 3$ and $x = 4$ K-doped C_{60} MLs. In particular, we believe that the JT effect and the intermolecular Coulomb interaction act cooperatively. For an even number of electrons, the JT effect suppresses intermolecular electron itinerancy (via Pauli exclusion) and hence reduces metallic screening. Worsened screening then enhances intramolecular charging energy (*6*, *26*, *27*) and thus enhances electron localization. Increased electronic localization, in turn, favors JT distortion (by reducing electron-number fluctuation on each molecule), causing a feedback cascade that results in an insulating K_4C_{60} ML ground state.

Two possible mechanisms might lead to the rearrangement of orientation seen in the insulating K_4C_{60} ML. The first involves quadrupole-quadrupole interactions between charged C_{60} molecules. Our DFT calculation indicates that JT distorted C_{60}^{4-} has a quadrupole moment of order $1|e|$ Å^2, where e is the electron charge. The ordering of C_{60} orientation seen in Fig. 3 is indeed favored by the quadrupolar interaction, but the energy difference between the observed structure and other metastable structures is small (on the order of 1 meV per molecule). Another possible mechanism for the order of orientation seen in Fig. 3 results from the anisotropic electronic overlap integral between molecules (*6*, *28*). Because the highest occupied molecular orbitals peak near the C_{60} pentagons, one intuitively expects direct pentagon-pentagon intermolecular alignment to enhance intermolecular overlap and reduce electronic kinetic energy. Indeed, for the order of orientation seen in Fig. 3, three of four equatorial pentagons per molecule face a pentagon from a neighboring molecule. A better understanding of the observed C_{60} arrangement and detailed spectroscopic features will likely have to include interaction of the molecules with the K ions and with the Au substrate, as well as quasiparticle effects that go beyond DFT in the standard local-density approximation.

References and Notes

1. R. C. Haddon *et al.*, *Nature* **350**, 320 (1991).
2. R. F. Kiefl *et al.*, *Phys. Rev. Lett.* **69**, 2005 (1992).
3. F. Stepniak, P. J. Benning, D. M. Poirier, J. H. Weaver, *Phys. Rev. B* **48**, 1899 (1993).
4. A. F. Hebard *et al.*, *Nature* **350**, 600 (1991).
5. W. L. Yang *et al.*, *Science* **300**, 303 (2003).
6. O. Gunnarsson, *Alkali-Doped Fullerides: Narrow-Band Solids with Unusual Properties* (World Scientific, River Edge, NJ, 2004).
7. H. A. Jahn, E. Teller, *Proc. R. Soc. London Ser. A* **161**, 220 (1937).
8. R. Kerkoud *et al.*, *J. Phys. Chem. Solids* **57**, 143 (1996).
9. P. Durand, G. R. Darling, Y. Dubitsky, A. Zaopo, M. J. Rosseinsky, *Nat. Mater.* **2**, 605 (2003).
10. Y. Iwasa, T. Takenobu, *J. Phys. Cond. Matter* **15**, R495 (2003).
11. V. Brouet, H. Alloul, S. Garaj, L. Forro, *Struct. Bonding* (*Berlin*) **109**, 165 (2004).
12. P. Paul, Z. W. Xie, R. Bau, P. D. W. Boyd, C. A. Reed, *J. Am. Chem. Soc.* **116**, 4145 (1994).
13. M. Fabrizio, E. Tosatti, *Phys. Rev. B* **55**, 13465 (1997).
14. L. F. Chibotaru, A. Ceulemans, S. P. Cojocaru, *Phys. Rev. B* **59**, R12728 (1999).
15. J. E. Han, E. Koch, O. Gunnarsson, *Phys. Rev. Lett.* **84**, 1276 (2000).
16. M. Capone, M. Fabrizio, P. Giannozzi, E. Tosatti, *Phys. Rev. B* **62**, 7619 (2000).
17. P. Dahlke, M. J. Rosseinsky, *Chem. Mater.* **14**, 1285 (2002).
18. K. Kamaras *et al.*, *Phys. Rev. B* **65**, 052103 (2002).
19. L. H. Tjeng *et al.*, *Solid State Commun.* **103**, 31 (1997).
20. C. Cepek, M. Sancrotti, T. Greber, J. Osterwalder, *Surf. Sci.* **454**, 467 (2000).
21. Our experiments were performed using a home-built ultrahigh vacuum STM cooled to 7 K. A polycrystalline PtIr tip was used for all measurements. C_{60} was dosed at coverages between 80% ML and 90% ML onto a clean Au(111) substrate cooled to 80 K. C_{60} coverages were determined from STM images. K was deposited progressively from a calibrated K getter onto the cooled C_{60} sample, followed each time by an anneal at 490 ± 10 K for 15 min. K getters were manufactured by SAES Getters (Milan, Italy), and calibrated by deposition of K on a clean Ag(100) substrate cooled to 80 K and counting single K atoms in topographic STM images acquired at 7 K. Local electronic structure was measured through STM *dI/dV* spectra acquired using standard lock-in techniques under open-loop conditions.
22. A. Ceulemans, *J. Chem. Phys.* **87**, 5374 (1987).
23. N. Koga, K. Morokuma, *Chem. Phys. Lett.* **196**, 191 (1992).
24. N. Manini, E. Tosatti, A. Auerbach, *Phys. Rev. B* **49**, 13008 (1994).
25. J. Junquera, Ó. Paz, D. Sánchez-Portal, E. Artacho, *Phys. Rev. B* **64**, 235111 (2001).
26. X. H. Lu, M. Grobis, K. H. Khoo, S. G. Louie, M. F. Crommie, *Phys. Rev. B* **70**, 115418 (2004).
27. R. Hesper, L. H. Tjeng, G. A. Sawatzky, *Europhys. Lett.* **40**, 177 (1997).
28. O. Gunnarsson, S. Satpathy, O. Jepsen, O. K. Andersen, *Phys. Rev. Lett.* **67**, 3002 (1991).

29. This work was supported in part by the Director of the Office of Energy Research, Office of Basic Energy Science, Division of Material Sciences and Engineering, U.S. Department of Energy under contract no. DE-AC03-76SF0098 and by NSF grant no. DMR04-39768. Y.W. thanks the Miller Institute for a research fellowship.

Supporting Online Material

www.sciencemag.org/cgi/content/full/310/5747/468/DC1
SOM Text
Fig. S1

12 July 2005; accepted 9 September 2005
10.1126/science.1117303